Online Li-ion battery state of health implementation for grid-tied applications

Irene Peláez
Electrical Engineering Dept.
University of Oviedo
Gijon, Spain
pelaezirene@uniovi.es

Ramy Georgious
Electrical Engineering Dept.
University of Oviedo
Gijon, Spain
georgiousramy@uniovi.es

Sarah Saeed
Electrical Engineering Dept.
University of Oviedo
Gijon, Spain
saeedsarah@uniovi.es

Pablo García
Electrical Engineering Dept.
University of Oviedo
Gijon, Spain
garciapablo@uniovi.es

Igor Cantero
R&D Dept.
CEGASA Energía
Vitoria, Spain
icantero@cegasa.com

***Abstract*—This paper introduces an online method valid to estimate the state of health of Li-ion energy storage systems for grid-tied applications. For this propose, two methods are evaluated. Firstly, a reduced-range incremental capacity analysis (ICA) applied during the last phase of the charging period (above 60-100% approximated) is analyzed, and also, an implementation strategy is proposed. This method has been successfully tested using data gathered during the degradation process of six LFP battery cells of 180 Ah and 100 Ah. However, it requires the energy storage system to be operated up to full charge. For overcoming that limitation, a second method based on adaptive filtering techniques to estimate the impedance evolution at different operating points is also studied. The proposed impedance-based method is analyzed using the data gathered from a cycling test.**

***Index Terms*—Lithium batteries, Adaptive estimation, Impedance, Prognostics and health management**

I. Introduction

Energy storage in stationary applications, particularly those using battery-based storage systems, shows an increasing interest [1]. Within the battery alternatives, $LiFePO_4$ chemistry (LFP) is a strong competitor for these kind of applications [2]. However, battery degradation due to high-demanding power profiles has a strong impact on the overall system reliability [3]–[5]. Considering that, a robust health indicator of the battery, widely known as the state of health (SoH), is highly acclaimed [6].

Several factors lead to battery degradation, where very high/low temperature, state of charge (SoC) limits excess and high current rates (C_r) have the highest contribution to a shorten lifespan [6]. These factors boost the degradation processes that take place in the inner cell, which mainly are loss of lithium inventory and loss of active materials [7]. Focusing on the inner elements of a cell, the negative electrode, usually made with graphite, becomes the one that most suffers during the degradation process [8]. This is mainly due to the solid electrolyte interphase (SEI) formation, which is a film that covers the negative electrode, generated when the electrode is exposed to the electrolyte [6], [8]. Finally, battery degradation becomes noticeable in its performance, and this deterioration results in a higher impedance and capacity loss [6]–[8]. For SoH estimation, these two parameters are of extreme interest.

This paper seeks to analyze the conditions to obtain an accurate SoH estimation, which relates the current nominal capacity (Q_n) with the initial one ($Q_{n\,ini}$). There is no method capable to fulfill the performance requirements of the battery model [9] and predict its life [8]. Several online and offline methods have been proposed to estimate the SoH and most of them require an accurate track of the inner impedance [10]. This impedance tracking method has also been used for SoC estimation proposes [11]. Unfortunately, a battery has a very non-lineal performance and it results difficult to determine the impedance rise due to degradation since it is also coupled with temperature, current and state of charge (SoC).

Under test conditions, incremental capacity analysis (ICA) helps to understand the degradation process of the battery [7]. This test analyzes the capacity increment (dQ_{BAT}) with the voltage increment (dV_{BAT}). An LFP cell has a set of constant voltage ranges derived from the physical insertion of the lithium ions into the graphite structure layers. These constant voltage ranges result in peaks when analyzing the correlation between dQ_{BAT} respect to dV_{BAT} [5], [7], [12]. The peaks tend to vary with aging: they are displaced to the right due to a higher impedance and the area of the peaks is

The present work has been partially supported by the predoctoral grant programs Severo Ochoa for the formation in research and university teaching of Principado de Asturias PCTI-FICYT under the grant ID BP16-133. This work also was supported in part by the European Union's H2020 Research and Innovation programme under Grant Agreement No 864459 (UE-19-TALENT-864459).

altered. However, the current rate affects the peak number: five peaks can be observed under low constant currents rates (C_r) [5], [7], whereas only three can be noticed at constant $C_r/3$ charge [12]. This C_r is typical for the charging process, making this method attractive for this application [12].

The present paper is structured as follows. In Section II, the cycling test performed to different cells is explained under detail. In Section III, the ICA analysis proposed and its implementation is exposed. In Section IV, the results of tracking the internal impedance are presented. Finally, the main conclusions of the paper are summarized in Section V.

II. Battery Cycling Test

Firstly, the evolution of the SoH (1) under laboratory conditions is analyzed. For that propose, three sets of cycles have been performed for each of the two different types of cells described in Table I. The tests proposed have been carried out in Cegasa Energía company using the cycler Digatron MCT 200-06-2 under the conditions gathered in Table II. The battery cell is cycled from the minimum to the maximum voltage value recommended in the datasheet, while the state of charge (SoC) is measured by using Coulomb counting (2), from the beginning (t_0) to the end (t_f) of the cycle. Due to the integration procedure, errors in Coulomb counting can become noticeable with time. For tackling this issue, the SoC is reset to zero when the cell reaches the minimum voltage. Fig. 1 depicts a set of cycles for one of the example tests. The voltage, current, and temperature profiles measured are depicted in Fig 1a,b,d, respectively. The SoC calculated is showed in Fig. 1c. When the cell charge is completed, a cycle is counted as shown in Fig. 1e.

$$SoH[\%] = \frac{Q_n(25^oC, 0.2C_r)}{Q_{n\,ini}} \cdot 100 \tag{1}$$

$$SoC_{BAT}[\%] = \frac{\int_{t_f}^{t_0} I_{BAT} dt}{Q_{n\,ini}} \cdot 100 \tag{2}$$

Table I
Test characteristics.

$\mathbf{Q}_{nom}$ [Ah]	$\mathbf{V}_n$ [V]	$\mathbf{Z}_{1000Hz}$ [m Ω]	$\mathbf{V}_{min}$-$\mathbf{V}_{max}$ [V]	$\mathbf{C}_r$ dis/ch	Cycles $C_r = 0.3$
180	3.2	0.6	2.5 - 3.65	0.3	2000
100	3.2	0.6	2.5 - 3.65	0.3	2000

Table II
Cell characteristics.

Test	100a	100b	100c	180a	180b	180c
$\mathbf{C}_{ch}$	0.5	0.75	1	0.5	1	1
$\mathbf{C}_{dis}$	0.5	0.75	1	1	1	1
T [° C]	40	40	40	40	40	20

At different stages of cycling, the test is stopped to evaluate the SoH. In order to avoid possible coupling effects of temperature and current rate (C_r), the criteria of the SoH test is the same one for all tests: a set of three cycles at a rate of $C_r/5$ with a cell temperature of 25^oC. The resulting SoH (1) is the mean of the previous three cycles and the evolution for the different cells is shown in Fig. 2. All of the tests have a clear dependency with cycling, wherein this case is the main contributor of aging.

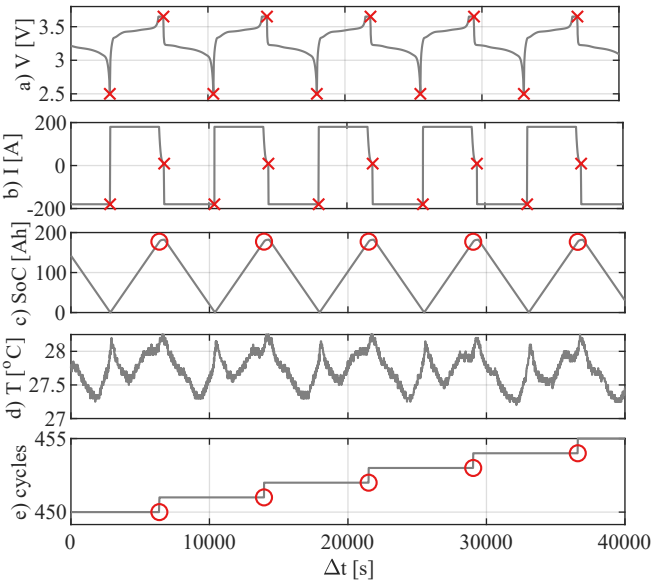

Figure 1. Time interval of Test 180c. Red crosses denotes when the resistance is measured. Circles denotes when a cycle is counted.a) Voltage profile. b) Current profile. c) SoC calculated. d) Temperature profile. e) Cycle counting.

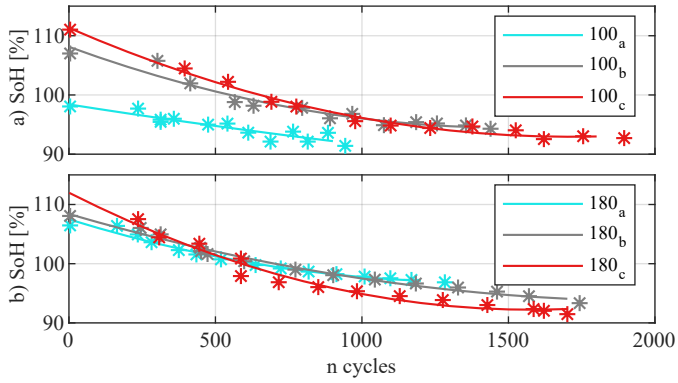

Figure 2. SoH evolution with cycling. a) 100 Ah case. b) 180 Ah case. The asterisk denotes the corresponded cycle when the capacity was measured.

III. Incremental Capacity Analysis - ICA

The ICA collects the relation between the increment of capacity with the increment of voltage, as shown in (3), along with the whole open-circuit voltage profile. A reduced range ICA implementation is proposed to analyze the previous cycling tests and it is valid for online implementation when

the battery is charged at this range. The target peak selected is the one obtained from the ICA test at the last constant voltage phase when charging the cell, which is likely to vary more [12]. Fig. 3a represents the charge evolution depending on the voltage. This constant voltage phase is reduced with aging, as shown in the highlighted rectangle, thus resulting in a reduced peak. The ICA correlation (3) of this example is represented in Fig. 3b, where the area of the target peak (P_a) becomes smoother as the constant voltage phase vanishes. Furthermore, this peak is displaced to the right due to the impedance variation. By tracking the peak displacement due to the impedance fluctuation [5], [7], it can be omitted their coupling effects in the resulting P_a, leading to an enhanced SoH estimation.

$$ICA_{BAT}[Ah/V] = \frac{\Delta Q_{BAT}}{\Delta V_{BAT}} \tag{3}$$

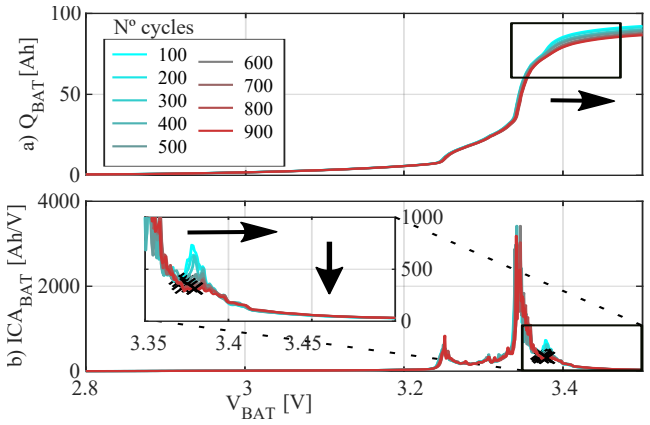

Figure 3. ICA curve evolution for the 100a Test. a) Q_{BAT} during a set of charge cycles. The section of the curve corresponding to the target peak is shown in a box. b) ICA curve evolution. The zoom shows the P_a for the target peak.

The P_a corresponded to the last charging peak has been tracked following the scheme proposed in Fig. 4. Initialization of the algorithm is done by looking for the I_x point, which is initially located in the vicinity of 60% SoC. Following, Q_{BAT} and V_{BAT} are filtered with a 2nd order zero-phase low pass filter (LPF) and a cutoff frequency 0.1 times the Nyquist frequency (fN), as shown in Fig. 4-1. In the second step (Fig. 4-2), both variables are re-sampled so evenly-spaced voltage data curves are obtained. Next, the ICA curve (3) is obtained filtered with the same previous filter (ICA_f), which is the one used for tracking the P_a as shown in the flowchart in Fig. 4. The minimum I_x between the two main peaks is located. If a minimum exists, then I_x is set to that point. If this peak vanishes due to aging, there is no local minimum anymore and the search is changed to look for the first inflection point to the right of the main peak, which will be considered as a valid I_x. Finally, P_a is calculated, which corresponds to the shaded area of the ICA_{BAT} curve in Fig 4-2.

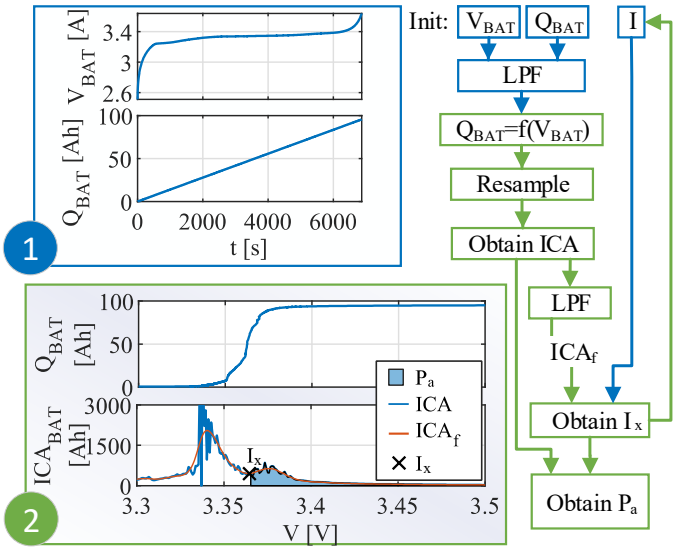

Figure 4. Signal processing proposed for the ICA implementation.

For the 100 Ah case, the test has been performed under the same temperature but different C_r. It is observed in Fig. 5, that the higher the current, the more shifted to the right the ICA curve. This is due to the voltage drop in the inner impedance, which increases with C_r. Besides, it can be observed how the target P_a decrements with aging in all cases. On the other hand, the 180 Ah cell is cycled at different temperatures and C_r which also results in a shift on the ICA curve.

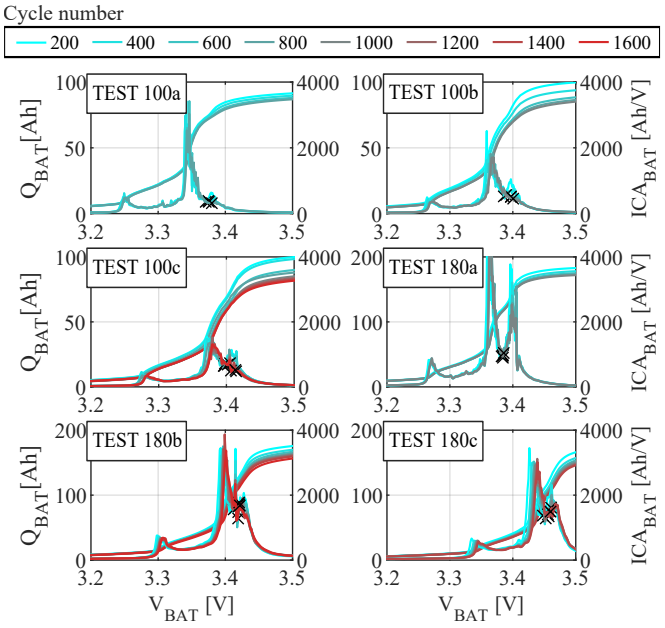

Figure 5. ICA results. Each plot has the capacity and the ICA curve evolution with voltage every 200 cycles.

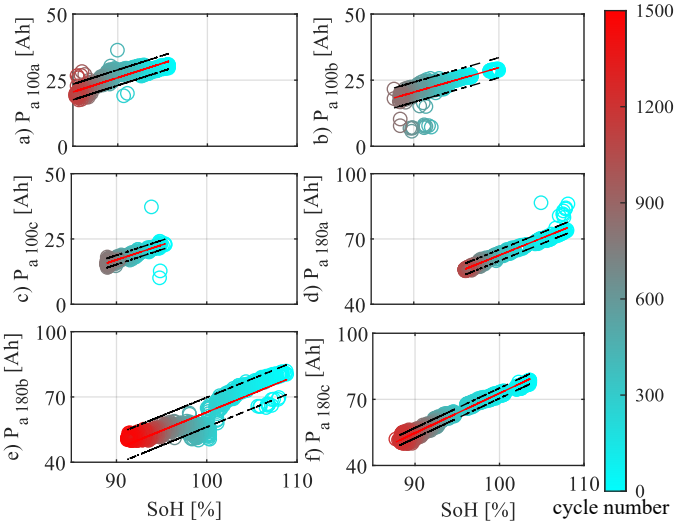

Figure 6. Relation of P_a with SoH for all cases. The red line represents the linear trend with coefficients gathered in Table III and the black lines shows the 2σ boundary. The data color reflect the number of cycle following the relation of the right bar.

Besides the ICA shifting, it has to be observed how the P_a varies with aging. As shown in Fig. 6, the evolution of P_a is lineal with SoH. Thus, a linear approach can be taken for all cases, which coefficients are defined in Table III. For the 100 Ah case, the P_a-SoH relation is quite similar for all situations. The same conclusions have been obtained for 180 Ah test cases, although the relation is different from the 100 Ah case. Good sensibility and analogous slopes for each capacity test are obtained. Thus, the proposed linear relationships can be used as a reference value each time the battery has a full charge and the ICA curve is calculated. For the ICA method to work accurately, mitigating the voltage drop disturbance at the internal impedance, the maximum recommended C_r for charging both battery cells is 0.5. In the shown tests, the C_r value has been always kept below that limit.

Table III
COEFFICIENTS OF THE SOH APPROXIMATION: $P_a = m\,SOH + b$

Test	m	b
100 a	1.1	-86
100 b	0.9	-56
100 c	0.9	-53
180 a	1.6	-95
180 b	1.7	-106
180 c	1.8	-107

IV. ONLINE IMPLEMENTATION

For the online implementation, it is proposed to use the internal resistance evolution with SoH as a figure of merit and see the coupling effects regarding the temperature. Two methods are proposed to analyze the estimated series resistance. The first method performs a linear regression (LR) of the last data recorded and does not have a forgetting factor. This method requires of extra memory in the online implementation. The second method uses a recursive least square (RLS) filter which does not require to record a data window due to the forgetting factor (λ). This filter is implemented as presented in Algorithm 1.

Algorithm 1. Proposed RLS method.

λ_0; ▷ Initial forgetting factor
$P_0 = [v_1\, 0; 0\, v_2]$; ▷ Initial gain matrix
$x1 = SoH$; ▷ Input data
$y1 = R$;
for $k = 1, 2, 3...Rsamples$ **do**
  $y_k = y1(k)$;
  $X = [1\, x1(k)]$;
  $e_k = \hat{y_k}[1, 1] - W_{k-1\,RLS} X_{RLS}$;
  $g_k = P_{k-1} X_{RLS}[\lambda + X_{RLS}^T P_{k-1} X_{RLS}]$;
  $Pk = \lambda^{-1} P_{k-1} - g_k X_{RLS}^T \lambda^{-1} P_{k-1}$;
  $w_{RLS} = W_{k-1\,RLS} + e_k g_k$;
  $P_{k-1} = P_k$;
  $W_{k-1} = W_k$;

The resistance is measured every time there is a step in the current profile greater than $0.3C_r$, by dividing the voltage by the current, at the points indicated in Fig 1a-b. The cycling test has a sampling time (T_s) of 5s. Unfortunately, this T_s is not enough to include frequency dynamics in the response. The internal resistance will also include some of the dynamics at the low-frequency range (< 0.5 Hz) where the diffusion processes are dominant [14].

During the cycling tests, the currents steps occur at low and high SoH. Fig. 7 presents the different evolution of R_s for both cases of test 180c. It can be shown that the internal resistance not only varies with aging, but also with SoC and temperature. The rising resistance evolution with a lower SoH is more clear in the low SoC side. Besides, the temperature has an slight impact on the resistance, where for this temperature range is less appreciable than the aging impact.

Fig. 8 shows the relation of the resistance with SoH and temperature of the previous example. A first-order approximation fit (4) is performed to check the different trends. The coefficients of (4) for both SoC cases are collected in Table IV. In order to track the impedance, it would be better to use the resistance at low SoC since the SoH sensibility is higher and the temperature has a lower impact.

$$R_{fit}\,[m\Omega] = b_1 SoH + b_2 T + b_0 \tag{4}$$

Table IV
COEFFICIENTS OF THE RESISTANCE FITTING: $R_{fit} = B_1\,SOH + B_2 T + B_0$

Test	b_0	b_1	b_2
$\mathbf{R}_{LowSoC}$	1.4104	-0.0098	-0.0036
$\mathbf{R}_{HighSoC}$	0.1718	-0.0014	0.0021

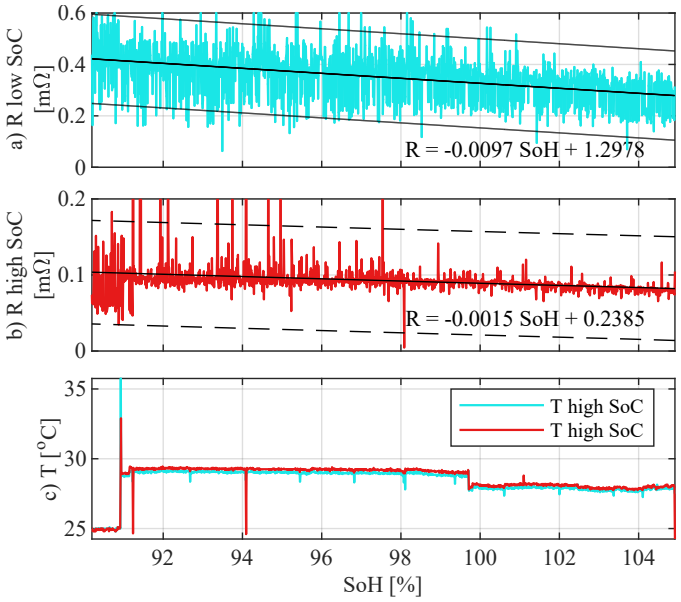

Figure 7. Test 180c. Relation of R_a with SoH. The blue line represents the low SoC case and the red line the high one. The black line denotes the lineal fit and the dashed line represents $\mp 2\sigma$ limits, that encloses 95% of the data.

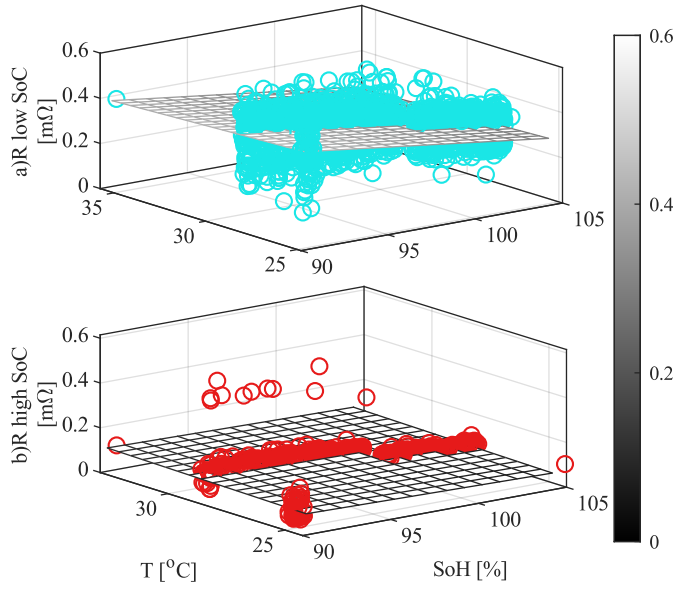

Figure 8. Relation of R_a with SoH and temperature of test 180c. a) Low SoC case. b) High SoC case.

Once the relation between the resistance and the temperature has been obtained, its effect can be decoupled by subtracting the temperature relation of (4). Fig. 9a shows the resistance (R1) without temperature effects. The two tracking techniques are used to find the coefficients of the resistance evolution using the theoretical SoH and R_1 as an input. For the LR, a window of the last 200 resistance samples are used. The RLS filter uses a λ of 0.999 and a gain matrix (P), with initial variance coefficients v_1 and v_2 set to 10^3 and 10^6, respectively.

Once the temperature relation is founded, their effects can be decoupled by subtracting the linear temperature relation gathered in Table. IV. Fig. 9a has the new resistance (R_1) without temperature effects. The two tracking techniques are used to find the coefficients of the resistance evolution using the SoH and R_1 as an input. For the LR, a window of the last 200 resistance samples are used. The RLS filter uses a λ of 0.999 and a gain matrix (P), with initial variance coefficients v_1 and v_2 set to 10^3 and 10^6, respectively.

In Fig. 9b-c, it can be observed the improvement in the coefficient tracking when using the RLS filter. The reference coefficients (Ref) correspond to the ones gathered in Table IV for the low SoC case. Notice the RLS filter performs better and smoother estimations. The LR technique does not start until the data window is completely full. The estimated resistance tracking is compared with the real one in Fig. 9d. If it is considered the estimated coefficients with the input resistance, the SoH can be estimated as shown in Fig. 9e. The RLS filter becomes a better estimator than the LR one, although it requires acquiring resistance measures to let the coefficients properly converge.

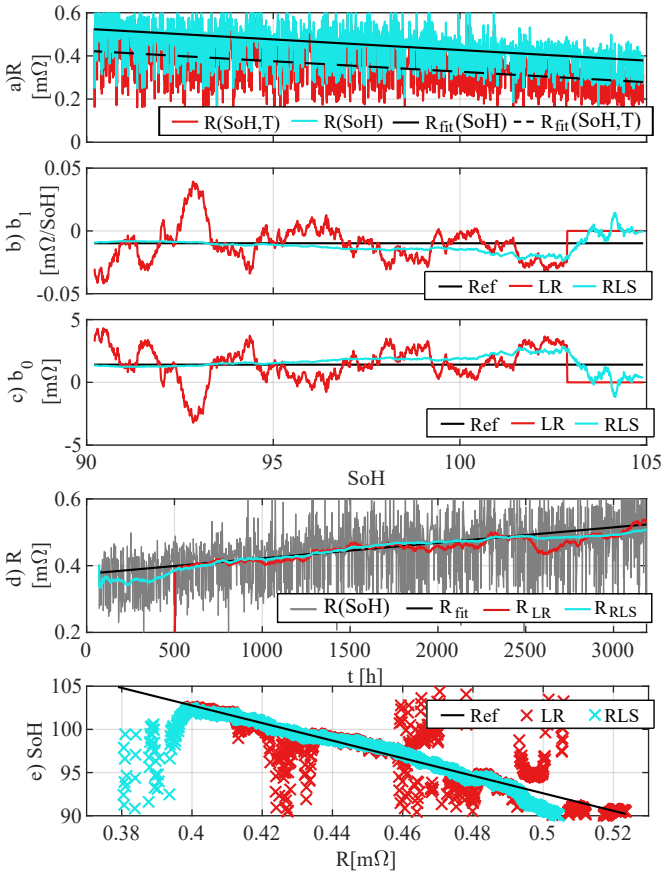

Figure 9. R tracking implementation results. a) R with and without T effects. The second one is used in the tracking techniques. b) b_1 coefficient tracking (4). c) b_0 coefficient tracking (4). d) Resulting resistance tracking with the estimated coefficients (4). e) SoH estimation using both techniques.

The inverse relation of SoH in terms of R using the fit vector is shown in (5). However, this inner resistance has to be characterized for each cell case which makes the resistance tracking complicated to generalized when compared to the

first ICA method. Here, actual research efforts are directed to obtain a combination of both ICA and impedance-based methods to enhance the SoH estimation.

$$SoH_{180_c} = -101.7135R[m\Omega] + 143.4541 \quad (5)$$

V. Conclusions

In the present work, two different forms of aging identification have been evaluated. ICA method has obtained very good results with different currents rates usually above the limited ones, and a similar aging trend has been found when analyzing the peak of the ICA curve at the last stage of the charge. Thus, the method could be applied in real-time applications considering variable load profiles. However, if the charging process does not cover the 60-100% charge stage with limited current derivatives, the ICA curve cannot be evaluated anymore. Thus, a method based on the internal resistance has been also proposed. Two main conclusions are drawn: 1) the internal resistance is very susceptible to temperature variation and 2) it has a higher sensibility to SoH variations at lower SoC, making this range more interesting for the implementation. The resistance temperature dependency has been decoupled based on the gathered lab data, and the decoupled resistance estimation has been used as the input of two different tracking online techniques: the linear regression and a RLS filter. The second technique results in a better option due to a smaller memory footprint and a lower error in the estimation. However, the resistance track needs for a previous commissioning process at the different cells, showing a lower generalization than the ICA alternative. Fusion methods using both techniques are currently a field of active research by the authors.

References

[1] S. Ci, N. Lin, and D. Wu, "Reconfigurable battery techniques and systems: A survey," *IEEE Access*, vol. 4, pp. 1175–1189, 2016.

[2] T. D. L. N. Tsiropoulos, I., "Li-ion batteries for mobility and stationary storage applications – scenarios for costs and market growth," no. JRC113360, 2018.

[3] M. D. Beirão, M. d. R. A. Calado, J. A. N. Pombo, and S. J. P. S. Mariano, "Balancing management system for improving li-ion batteries capacity usage and lifespan," in *2016 IEEE 16th International Conference on Environment and Electrical Engineering (EEEIC)*, June 2016, pp. 1–6.

[4] J. Li, S. Zhou, and Y. Han, *Recent Research on battery diagnostics, prognostics, and uncertainty management*. IEEE, 2017, pp. 175–216. [Online]. Available: https://ieeexplore.ieee.org/document/7656894

[5] D. Anseán, V. M. García, M. González, C. Blanco-Viejo, J. C. Viera, Y. F. Pulido, and L. Sánchez, "Lithium-ion battery degradation indicators via incremental capacity analysis," *IEEE Transactions on Industry Applications*, vol. 55, no. 3, pp. 2992–3002, May 2019.

[6] J. Vetter, P. Novák, M. Wagner, C. Veit, K.-C. Möller, J. Besenhard, M. Winter, M. Wohlfahrt-Mehrens, C. Vogler, and A. Hammouche, "Ageing mechanisms in lithium-ion batteries," *Journal of Power Sources*, vol. 147, no. 1, pp. 269 – 281, 2005. [Online]. Available: http://www.sciencedirect.com/science/article/pii/S0378775305000832

[7] M. Dubarry and B. Y. Liaw, "Identify capacity fading mechanism in a commercial lifepo4 cell," *Journal of Power Sources*, vol. 194, no. 1, pp. 541 – 549, 2009, xIth Polish Conference on Fast Ionic Conductors 2008. [Online]. Available: http://www.sciencedirect.com/science/article/pii/S0378775309009604

[8] G. Plett, *Battery Management Systems, Volume II: Equivalent-Circuit Methods*, ser. Artech House power engineering series. Artech House, 2015.

[9] M. Cacciato, G. Nobile, G. Scarcella, and G. Scelba, "Real-time model-based estimation of soc and soh for energy storage systems," *IEEE Transactions on Power Electronics*, vol. 32, no. 1, pp. 794–803, Jan 2017.

[10] F. A. Shah, S. Shahzad Sheikh, U. I. Mir, and S. Owais Athar, "Battery health monitoring for commercialized electric vehicle batteries: Lithium-ion," in *2019 International Conference on Power Generation Systems and Renewable Energy Technologies (PGSRET)*, Aug 2019, pp. 1–6.

[11] P. García, . Navarro-Rodríguez, S. Saeed, and J. García, "Soc estimation in li-ion batteries exploiting high-frequency model properties," in *2018 IEEE Energy Conversion Congress and Exposition (ECCE)*, Sep. 2018, pp. 1103–1110.

[12] E. Riviere, A. Sari, P. Venet, F. Meniere, and Y. Bultel, "Innovative incremental capacity analysis implementation for c/lifepo4 cell state-of-health estimation in electrical vehicles," *Batteries*, vol. 5, no. 2, 2019. [Online]. Available: https://www.mdpi.com/2313-0105/5/2/37

[13] A. Lievre, A. Sari, P. Venet, A. Hijazi, M. Ouattara-Brigaudet, and S. Pelissier, "Practical online estimation of lithium-ion battery apparent series resistance for mild hybrid vehicles," *IEEE Transactions on Vehicular Technology*, vol. 65, no. 6, pp. 4505–4511, June 2016.

[14] M. Xiao and S.-Y. Choe, "Impedance model of lithium ion polymer battery considering temperature effects based on electrochemical principle: Part i for high frequency," *Journal of Power Sources*, vol. 277, pp. 403 – 415, 2015. [Online]. Available: http://www.sciencedirect.com/science/article/pii/S0378775314017765

[15] R. B. G. R. D. B. Marcello Torchio, Lalo Magni and D. M. Raimondo, "Lionsimba: A matlab framework based on a finite volume model suitable for li-ion battery design, simulation, and control," *Journal of the Electrochemical Society*, vol. 163, no. issue 7, pp. A1192–A1205., 2016.

[16] I. Peláez, P. García, G. Villa, and S. Saheed, "Li-ion batteries parameter estimation using converter excitation and fusion methods," in *2019 IEEE Energy Conversion Congress and Exposition (ECCE)*, Sep. 2019, pp. 2491–2498.